Absolute low-energy e^--Ar scattering cross sections

J. E. Furst and D. E. Golden
Department of Physics and Center for Materials Characterization, University of North Texas, Denton, Texas 76203

M. Mahgerefteh
Department of Physics and Center for Materials Characterization, University of North Texas, Denton, Texas 76203 and Department of Physics and Astronomy, Portland State University, Portland, Oregon 97207

Jiaxiang Zhou
Department of Physics and Center for Materials Characterization, University of North Texas, Denton, Texas 76203 and Department of Physics and Astronomy, University of Oklahoma, Norman, Oklahoma 73069

D. Mueller
Department of Physics and Center for Materials Characterization, University of North Texas, Denton, Texas 76203
(Received 26 June 1989)

Relative measurements of e^--Ar angular distributions in the energy range 3–20 eV have been placed on an absolute scale by both a phase-shift analysis and relative flow normalization. The two sets of absolute differential cross sections are in excellent agreement with each other over the entire energy range. These measurements are also in agreement with previous calculations and measurements in different energy and angular ranges. Total cross sections calculated from the derived phase shifts are in excellent agreement with recent direct experimental determinations.

INTRODUCTION

Rare-gas atoms provide a useful reference for the measurement and calculation of atomic properties. In addition, the practical development and modeling of systems such as rare-gas–halide lasers has indicated a need for more accurate information on electron-atom collision processes.

Since the direct determination of absolute cross sections is exceptionally difficult, the most common approach to this goal is to measure relative differential cross sections and then place them on an absolute scale by normalization to cross sections for targets for which the absolute cross sections are well known. At sufficiently low energies, where only elastic scattering occurs, phase shifts for some of the lowest-order partial waves may be obtained by fitting angular distribution measurements.[1] These extracted phase shifts, together with higher-order phase shifts given by the Born approximation, for example, may be used to place differential cross sections on an absolute scale. The latter method has been used extensively in helium and provides the standard for e^--He absolute differential cross-section measurements at low energies.

The results of such measurements for energies from 2 to 19 eV have been summarized by Golden, Furst, and Mahgerefteh.[2] A similar analysis has been used to extract phase shifts from elastic angular distributions measured in argon by Andrick,[3] Williams,[4] and Srivastava *et al.*[5] However, phase-shift analysis as a method of determining absolute differential cross sections in argon has thus far been less successful than in helium and most argon measurements have been placed on an absolute scale by some type of normalization to measurements in helium. Total cross sections obtained by phase-shift analysis of relative angular distribution measurements by Srivastava *et al.*[5] are consistently higher, by as much as 60%, than total cross sections obtained by them from relative flow normalization of such measurements. This has thrown both phase-shift analysis and relative flow normalization techniques into question. While angular distributions have been measured by a number of authors,[3–7] recent measurements of differential cross sections in argon show substantial differences in the absolute cross sections (up to about 50%) and the positions of the prominent minima present in the low-energy range (up to about 45%).

For a heavy rare-gas atom such as argon, the validity of a phase-shift analysis at any energy is not generally accepted. The polarizability of argon is much larger than that of helium, so higher-order partial waves contribute significantly to the scattering cross sections at any energy. The effect of these higher-order phases is to cause a sharper forward peak in the differential cross sections. In addition, the relatively large d-wave contribution creates two distinct minima in the differential cross sections at low energies, with the d wave becoming more dominant as the energy increases. The validity of using the Born approximation for the higher-order phase shifts, even at relatively low energies, is called into question. It is also possible to place the differential cross sections on an absolute scale by normalization to known helium differential cross sections using a relative flow technique.[8,9] Thus e^--Ar relative differential cross section

measurements can provide a direct comparison between the two methods. Indeed, such a comparison might define limits for the use of phase-shift analysis to obtain absolute differential cross sections.

In recent years there have been several total elastic cross-section measurements made in argon which have been summarized by Buckman and Lohmann.[10] The general agreement between the various total cross-section measurements provides some basis for judging between various methods used to place differential cross sections on an absolute scale. However, the angular range used in the measurement of differential cross sections can limit the accuracy of total cross sections derived from them. It is perhaps even more important to note that various angular distributions can give rise to the same total cross section because some parts of the angular distribution may have dominant contributions to the total cross section. For example, two angular distributions, one of which contains very sharp dips at small and large angles and the other of which has the same dips, but much less pronounced, may not differ markedly in the total cross section.

This paper reports measurements of absolute differential cross sections for electron scattering from argon in the energy range 3–20 eV using a time-of-flight technique described previously.[2] In the present work, relative differential cross section measurements in the angular range 20°–130° have been placed on an absolute scale using phase-shift analysis[1] and relative flow normalization techniques.[8,9] The time-of-flight technique used in this work provides an excellent means for discriminating against scattering events not due to the argon target beam. Most importantly, elastic scattering from the area surrounding the scattering region and electrons coming directly from the electron gun are easily discriminated against. In addition, the scattering geometry and target-beam density have been chosen so that no scattering volume corrections are needed to obtain the relative differential cross sections. This enables us to do low-energy, small-angle measurements reliably. Finally, there is no electron optics in front of the detectors so that changing the target beam has a minimal effect on the collection efficiency of scattered electrons. Thus direct comparisons between different target gases may be readily made.

APPARATUS AND EXPERIMENTAL METHOD

The time-of-flight apparatus used in this work is shown schematically in Fig. 1 and has been described in a previous publication.[2] Since that time several aspects of the experiment have been reexamined and we have rebuilt some parts of the apparatus.

Briefly, a pulsed electron beam crosses a well-collimated argon beam. The arrival time spectra of the scattered electrons are measured as a function of scattering angle in the plane containing both incident and scattered electrons perpendicular to the argon beam, by a rotating detector while a stationary detector monitors the scattering from the background gas. The signal in the stationary detector is proportional to the product of the electron-beam current and background-gas density.

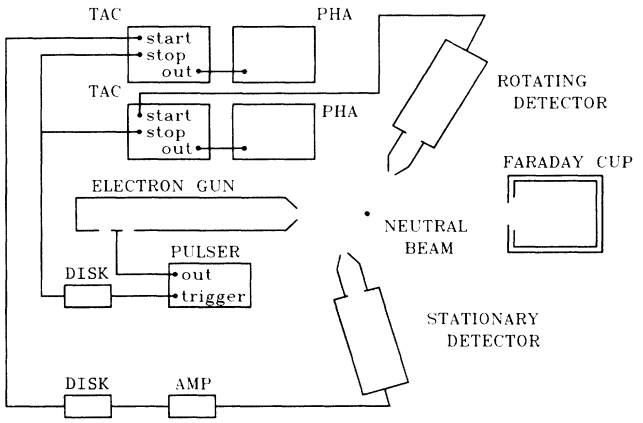

FIG. 1. Schematic diagram of the time-of-flight system.

Pulses from both the rotating and stationary detectors are processed by amplifiers (AMP) and discriminators (DISK) and then used to start time-to-amplitude converters (TAC). A trigger pulse from the pulser is processed through another DISK and then used to stop both TAC's. The TAC outputs are then pulse-height analyzed (PHA) and stored. Since the target-beam density is proportional to the background-gas density, normalizing the rotating detector signal to the stationary detector signal corrects for variations in the electron-beam current and the target-beam density. Following measurements with the argon beam on, the chamber is flooded to the same pressure as that of the background gas when the atomic beam was on. Then, normalized measurements using the flooded chamber are subtracted from normalized measurements with the target beam on in order to correct for the angular-dependent scattering from the background gas. The relative differential cross section $d\sigma(E,\theta)/d\Omega$ at a particular electron energy E and scattering angle θ is determined from

$$\frac{d\sigma(E,\theta)}{d\Omega} = k\,[R(E,\theta,\rho,I_e,V_i)/S(E,\theta,\rho_0,I_e,V_i') - R'(E,\theta,\rho_0,I_e,V_i)/S'(E,\rho_0,I_e,V_i')] = kN\ , \quad (1)$$

where k is a constant, R and S are, respectively, the scattering rates of the rotating and stationary detectors measured with the argon beam on, R' and S' are those rates with the argon beam off and the chamber flooded to the same background pressure as that when the gas beam was on, N is the normalized scattering rate, ρ and ρ_0 are the target-beam density and the background density, respectively, I_e is the electron-beam current, and V_i and V_i' are the interaction volumes viewed by the rotating detector at angle θ and the stationary detector, respectively. The rotating detector can make measurements in the angular range from $-35°$ to 135°. The entrance aperture to the rotating detector was 1.5 mm in diameter and that in the rotating detector was 2.0 mm for all the differential cross sections reported here. The solid angle subtended by the rotating detector was 1.13×10^{-2} sr. The target gas beam is formed inside a separately pumped chamber

by a 0.5-mm-diam molybdenum tube that is 50 mm long and skimmed by a sharpened 0.5-mm aperture, 2 mm from the end of the tube. Several measurements of the relative differential cross sections were made with entrance apertures in the rotating detector ranging in diameter from 0.5 to 2.0 mm. In this way we were able to estimate the diameter of the beam to be between 0.50 and 0.75 mm. This is roughly in agreement with the beam diameter estimate of 0.5 mm made previously.[1] The alignment of all mechanical parts relative to the target-beam direction was done using mechanical alignment rods and the alignment error for any one part is estimated to be less than 0.25 mm.

Each detector consisted of a 138-mm flight tube with dual microchannel plates in a chevron configuration. Two fine mesh copper grids were placed in front of the microchannel plates. The first was at ground potential to shield the interaction region from the electric field due to the detector bias voltage. The second grid was used as part of a retarding field energy analyzer to calibrate the electron-beam energy. A separate measurement of the 19.35-eV ^2S resonance in helium[2] was also used to calibrate the energy scale. We estimate the error in our energy calibration to be about 0.15 eV and the energy resolution to be about 0.3 eV. For the energy range covered in this work, there are two minima in the angular distribution that provide an excellent test of the angular resolution of the measurements. In this connection, it was important to establish the angular position accurately. Thus the position of zero angle has been determined using three methods. As the apparatus is being put together, the zero position is determined using the alignment tools. During normal operation, the zero position is determined by measuring the current collected in the rotating detector as a function of angle. For these measurements, the current is collected on the retarding grid with the microchannel plate high-voltage off. The electron-beam signal typically has a 3° full width at half maximum (FWHM) and falls off by three orders of magnitude at 10°. At several energies, the differential cross sections is small enough to allow these measurements to within 5° of zero so that the symmetry about the zero position can be determined. All three methods of determining the zero position are consistent with each other to about 0.2°. We estimate the maximum error in angle to be about 0.3°. This is comprised of 0.2° due to alignment and 0.1° due to reproducibility. Then, by making measurements at each minimum in the differential cross section and by using the rotating detector to establish the position of 0° scattering angle, the measured angular resolution of the apparatus was established to be $\pm 1.5°$.

Since low-energy electrons are easily deflected by stray electric or magnetic fields, special care was given to keep such fields in the interaction region to a minimum. Thus the interaction region has been carefully electrically shielded and all conducting surfaces near the interaction region have been constructed of oxygen-free high-conductivity copper and coated with colloidal graphite (Acheson Aerodag) in order to minimize surface effects. A combination of Molypermalloy magnetic shielding and square Helmholtz coils was used to minimize the magnetic fields at the electron gun, interaction region, and detectors. The magnetic field was measured to range from a low of 0.5 mG at the interaction region to a high of 1.5 mG at the end of the time-of-flight tube. The absence of stray fields was verified by the agreement of mechanical and measured beam zeros.

Since the validity of our assumption that the target-beam shape is independent of target-gas density requires the beam density to be sufficiently low, it was important to examine the relationship between the beam driving pressure and the resulting relative differential cross section. We did this for driving pressures between 0.3 and 3.5 Torr at several energies and angles. These driving pressures correspond to pressures that range from 1.0×10^{-7} to 5×10^{-7} Torr on the far side of the scattering chamber. We found that the relative differential cross sections was constant for the range of driving pressures between 0.4 and 2.0 Torr (1.3×10^{-7} and 2.6×10^{-6} Torr in the scattering chamber). This pressure range also gave helium-beam densities which were sufficient to measure the differential cross sections at 90° for the relative flow measurements.

DATA ANALYSIS

The shape of the angular distribution at each energy has been fitted using a phase-shift analysis. This fitting procedure enabled us to extrapolate measured relative differential cross sections to 0° and 180° and place them on an absolute scale. The result of this process has been compared with the absolute argon cross-section values determined by the relative flow technique used in our previous work in H_2 (Ref. 8), and has been checked using the slightly different relative flow technique described by Nickel *et al.*[9]

Phase-shift analysis

To speed up the process used to determine phase shifts, our fitting program has been rewritten using the least-squares fitting routines of Press *et al.*[11] This provided a very fast fit to the data at a high level of accuracy so that Monte Carlo techniques could be used to estimate the errors in the phase shifts. The differential cross sections can be expressed in terms of phase shifts[1]

$$\frac{d\sigma(E,\theta)}{d\Omega}=(\tfrac{1}{4}E)\left[\left[\sum_{l=0}^{L}(2l+1)\sin(2\delta_l)P_l+2\sqrt{E}f_B^L\right]+\left[\sum_{l=0}^{L}(2l+1)(\cos2\delta_l-1)P_l\right]^2\right], \tag{2}$$

where δ_l is the phase shift, P_l the Legendre polynomial of the lth partial wave, and f_B^L is the sum of the remaining Born amplitudes given by

$$f_B^L=\pi\alpha\sqrt{E}\left[-\tfrac{1}{2}\sin(\tfrac{1}{2}\theta)-\sum_{l=1}^{L}P_l/(2l+3)(2l-1)\right], \tag{3}$$

where α is the dipole polarizability of the atom. We fit the first four phase shifts and determined the rest using the modified effective range theory (MERT) of O'Malley, Spruch, and Rosenburg,[12] which includes the effect of the long-range dipole force on electron-atom scattering:

$$\tan\delta_l = \pi\alpha d k^2/(2l+3)(2l+1)(2l-1) \ . \quad (4)$$

The use of the $L>3$ phase shifts calculated by Fon *et al.*,[13] or McEachran and Stauffer,[14] for example, instead of the MERT values causes a variation of less than 1% in the absolute value of the differential cross section at any of the energies considered in this experiment.

The $L=3$ phase shifts calculated using MERT are compared with those resulting from our curve fitting procedure in Table III below. The $L=3$ phase shifts determined in this work agree well with MERT at and below 10 eV. At the higher energies, where inelastic processes are present, the agreement is somewhat worse, although not enough to consider fitting the $L=4$ term.

The errors in the phase shifts and the absolute differential cross section have been estimated by fitting a series of curves that are randomly distributed within one standard deviation of the experimental relative differential cross-section curve. The number of curves needed is determined by the convergence of the error values and is typically 300 for the present data. This type of error analysis provides an interesting method for testing the validity of phase-shift analysis. In general, the more structure in the shape of the differential cross section, the more accurate phase-shift analysis becomes.

Relative flow normalization at a steady-state driving pressure

This relative flow technique has been described previously,[2] and has been used in the present work as the primary normalization technique. Briefly, gas flows into a large volume through a finely controlled leak valve and flows out of the volume through the capillary described above. The pressure in the large volume is measured with a baratron. As discussed above, in this work, the driving pressure is always adjusted to be in the molecular flow region where atom-atom collisions are insignificant in the capillary. Under such conditions, the flow of gas from the source gives rise to neutral beams with density profiles that are independent of the target beam used. Thus direct comparison of scattering count rates between gases may be made. Under these conditions, the pressure measured by the baratron is proportional to the target-beam density. The rotating detector viewing cone is sufficiently large so that the entire target beam is viewed at all scattering angles.

Helium and argon relative differential cross section measurements are made at 90° as a function of the neutral beam driving pressure p. To increase the precision of the normalization, N has been measured as a function of p. These measurements have been fitted to

$$N = k'[d\sigma(E,90°)/d\Omega]p \ , \quad (5)$$

where k' is a constant independent of the target beam. Relative values of $d\sigma/d\Omega$ are determined by measuring N as a function of p for each target and using a regression analysis to find $k'[d\sigma(E,90°)/d\Omega]$ in each case. An example of a set of measurements of this type is shown in Fig. 2 at 10 eV. A straight line can be fit to the argon data in region I, both gases obey Eq. (5). In region II, the argon flow is undergoing a transition and N is not proportional to the pressure, while for helium, N is still proportional to the pressure. In region III, while a straight line can be fit to the argon data, the derived argon cross section is a factor of 2 greater than the phase-shift analysis result. The differential cross section derived from the ratio of slopes of the lower argon line and the helium line is in excellent agreement with the phase-shift analysis result. All of the work reported here is for operating pressures in region I. Once the ratio of values of $d\sigma(E,90°)/d\Omega$ in argon and helium at a particular energy is determined, absolute helium cross sections at 90° measured in our previous work[1] are used to place the argon relative cross section measurements on an absolute basis.

Relative flow normalization when driving pressure measured as a function of time

This relative flow technique has been described by Nickel *et al.*[9] and has been used as a check on the calibration technique described in the previous section. The flow rate is determined by setting the controlled leak valve to a particular setting. With the controlled leak valve set, the gas inflow is stopped and the large volume is evacuated. Once the large volume has been evacuated, the gas inflow is started again and the rate of increase of pressure with time F is measured by the baratron. This process is repeated with the other gas to be used with the same controlled leak valve setting to determine F'. Since the relative flow rates in the two gases are proportional to

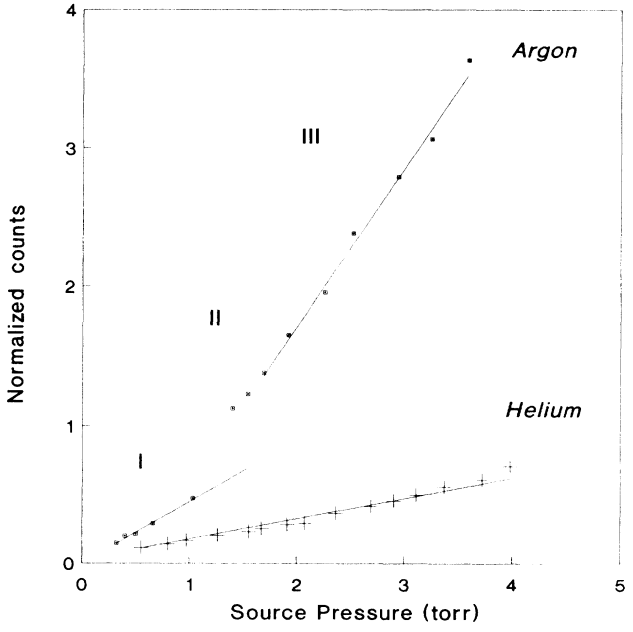

FIG. 2. Relative flow calibration as a function of pressure at 10 eV.

the rate of change of pressure in the large volume and inversely proportional to the square root of their masses, the relative differential cross sections measured at that same controlled leak valve setting are given by

$$\frac{N'}{N}=k'''\frac{I_e}{I_e'}\frac{d\sigma'(e,90°)}{d\Omega}\Big/\frac{d\sigma(E,90°)}{d\Omega}\frac{F}{F'}\left[\frac{m}{m'}\right]^{1/2}, \tag{6}$$

where m and m' are the masses of the two gases used in the calibration.

RESULTS AND DISCUSSION

Absolute differential cross sections, determined by phase-shift analysis at 3, 5, 10, 15, and 20 eV are plotted in Figs. 3–7, together with the errors determined using the Monte Carlo technique described in a previous section. The experimental results of Andrick,[3] Williams,[4] Srivastava *et al.*,[5] Dubois and Rudd,[6] and the calculations of Fon *et al.*,[13] McEachran and Stauffer,[14] and Ali and Fraser[15] are also shown on the figures. The present results have been determined from a series at least four measurements at each energy, so that the statistical error at each energy is less than ±2%. The measured positions of the minima in the differential cross section at 3, 5, 10, 15, and 20 eV, together with the results of Andrick,[3] Williams,[4] and Srivastava *et al.*[5] are summarized in Table I.

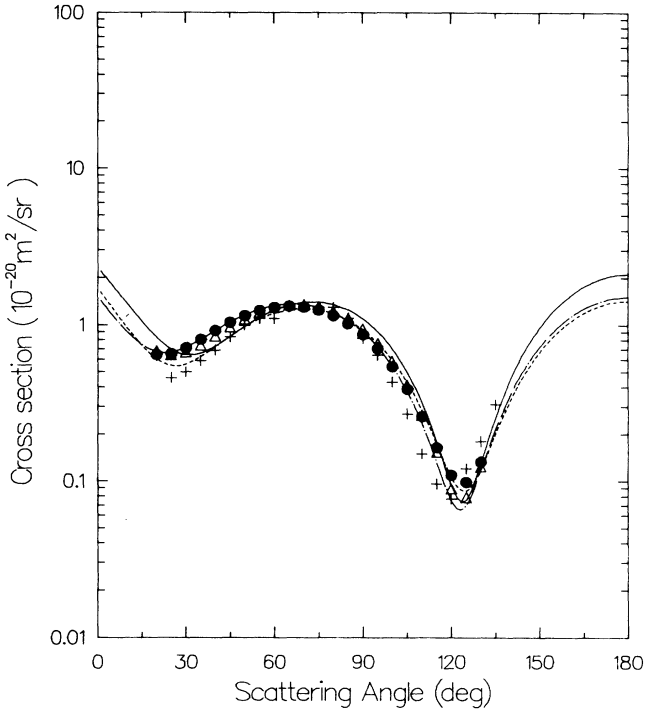

FIG. 4. Absolute differential scattering cross sections at 5 eV. ●, present work; △, Andrick (Ref. 3); +, Srivastava *et al.* (Ref. 5); —·—·—·, Fon *et al.* (Ref. 13); ——, McEachran and Stauffer (Ref. 14); — — —, Ali and Fraser (Ref. 15).

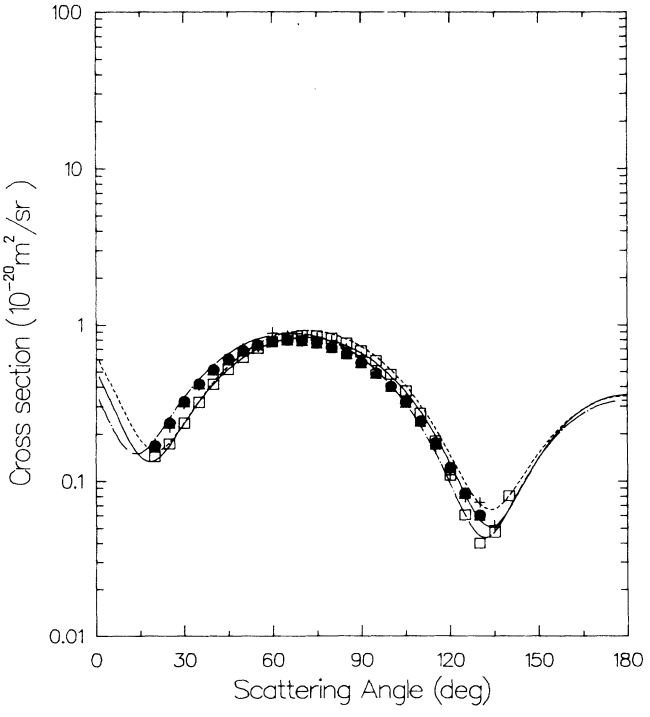

FIG. 3. Absolute differential scattering cross sections at 3 eV. ●, present work; △, Andrick (Ref. 3); □, Williams (Ref. 4); +, Srivastava *et al.* (Ref. 5); —·—·—·, Fon *et al.* (Ref. 13); ——, McEachran and Stauffer (Ref. 14); — — —, Ali and Fraser (Ref. 15).

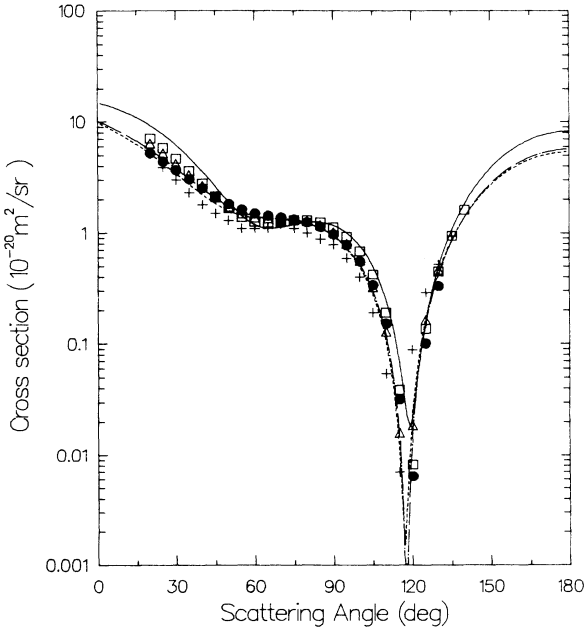

FIG. 5. Absolute differential scattering cross sections at 10 eV. ●, present work; △, Andrick (Ref. 3); □, Williams (Ref. 4); +, Srivastava *et al.* (Ref. 5); —·—·—·, Fon *et al.* (Ref. 13); ——, McEachran and Stauffer (Ref. 14); — — —, Ali and Fraser (Ref. 15).

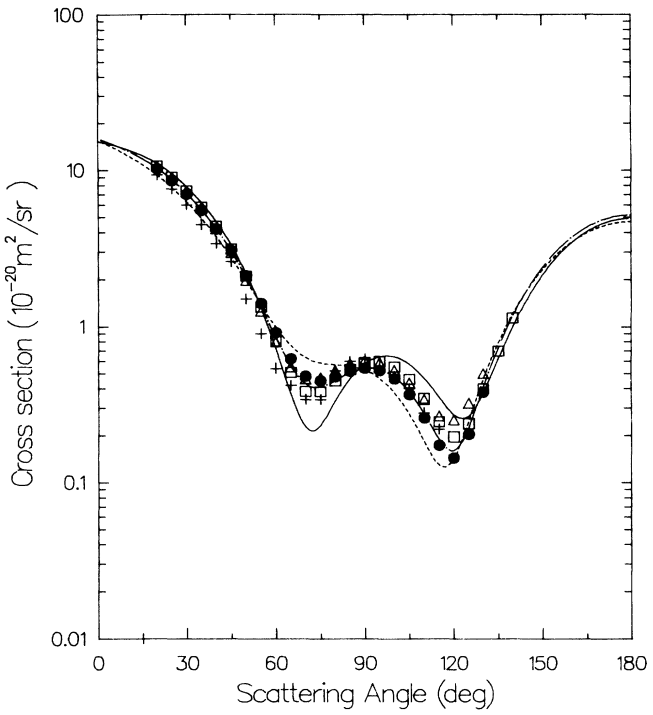

FIG. 6. Absolute differential scattering cross sections at 15 eV. ●, present work; △, Andrick (Ref. 3); □, Williams (Ref. 4); +, Srivastava *et al.* (Ref. 5); ◇, Dubois and Rudd (Ref. 6); ——, McEachran and Stauffer (Ref. 14); — — —, Ali and Fraser (Ref. 15).

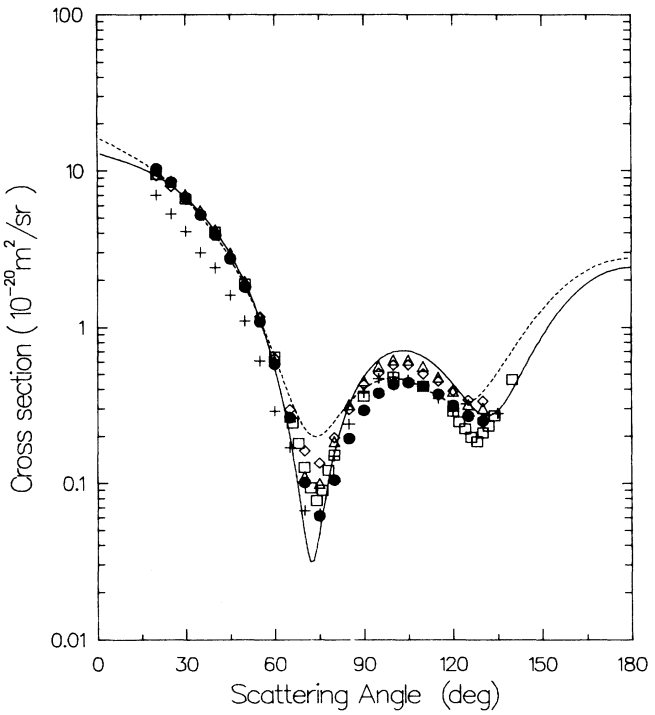

FIG. 7. Absolute differential scattering cross sections at 20 eV. ●, present work; △, Andrick (Ref. 3); □, Williams (Ref. 4); +, Srivastava *et al.* (Ref. 5); ◇, Dubois and Rudd (Ref. 6); ——, McEachran and Stauffer (Ref. 14); — — —, Ali and Fraser (Ref. 15).

TABLE I. Angles θ_1 and θ_2 corresponding to the first and second minimum in the argon scattering cross section.

E (eV)	θ_1 (deg)	θ_2 (deg)	Work
3	13[a]	135	Present
	15	135	Srivastava *et al.* (Ref. 5)
	14	132	Andrick (Ref. 3)
	19	131	Williams (Ref. 4)
5	21[a]	124	Present
	25	119	Srivastava *et al.* (Ref. 5)
	23	123	Andrick (Ref. 3)
10		118	Present
	60	115	Srivastava *et al.* (Ref. 5)
		117	Andrick (Ref. 3)
	64	119	Williams (Ref. 4)
15	75	119	Present
	70	117	Srivastava *et al.* (Ref. 5)
	73	120	Andrick (Ref. 3)
	72	120	Williams (Ref. 4)
20	74	130	Present
	73	128	Srivastava *et al.* (Ref. 5)
	73	129	Andrick (Ref. 3)
	74	127	Williams (Ref. 4)

[a]From phase-shift analysis.

At 3 eV, the present absolute differential cross sections lie on top of the previous measurements of Andrick[3] and Srivastava *et al.*[5] The present measurements also agree reasonably well with the results of Williams[4] at most angles, although the two sets of measurements disagree with each other by as much as 40% at several angles. The present results agree quite well with the calculations of Fon *et al.*[13] for angles between 30° and 90°, with the calculations of McEachran and Stauffer,[14] and Ali and Fraser,[15] for scattering angles of 60° and above.

At 5 eV, the present results are in good agreement with the results of Andrick.[3] However, between 20°–45° and 90°–130° the present results are quite different from those of Srivastava *et al.*[5] In the present work, the minimum in the backward direction is at 124°, while it is at 119° in the results of Srivastava *et al.*[5] In addition, the results of Srivastava *et al.*,[5] are lower by about 50% at some angles. Again, the calculations of Fon *et al.*[13] agree best with our data at small angles. The calculations of Ali and Fraser[15] and McEachran and Stauffer[14] agree best with our data for larger angles, although these calculations agree reasonably well with the present results over most of the angular range covered at this energy.

At 10 eV, the present results still agree quite well in shape with the results of Andrick[3] and Williams,[4] although differences in absolute value might be as large as 40% at some angles where the cross section is changing rapidly with angle. The present results disagree with the results of Srivastava *et al.*[5] over the full angular range. While the calculations of McEachran and Stauffer[14] show a minimum at about 60°, which is roughly in agreement with the minimum found by Srivastava *et al.*,[5] their differential cross sections do not agree well with either the present results or those of Srivastava *et al.*[5] The present results are in excellent agreement with the calculations of Fon *et al.*[13] and Ali and Fraser[15] over the entire range of the present measurements.

At 15 eV, the present results are in agreement with the measurements of Andrick[3] and Williams,[4] and agree to within 50% with the measurements of Srivastava *et al.*[5] The present results agree best with the calculations of Fon *et al.*[13] The calculations of Ali and Fraser[15] and McEachran and Stauffer[14] agree well with present measurement in the forward direction, but for larger angles there are significant differences between the shapes of the angular distributions and the positions of the minima.

At 20 eV, the present results are in excellent agreement with the previous measurements of Andrick,[3] Williams,[4] and Dubois and Rudd[6] for scattering angles less than 60°. For scattering angles above 60°, the present results are below these measurements by as much as a factor of 2. The present measurements are in reasonable agreement with the calculations of Ali and Fraser[15] and McEachran and Stauffer,[14] up to about 60°. At larger scattering angles, the shape of the present measurements agree with the shape given by these calculations, although there are differences in details that are as large as a factor of 2. The present measurements are as much as 30% above the previous measurements of Srivastava *et al.*[5] for scattering angles less than 70° and are in excellent agreement with them for scattering angles of 105° and greater.

The absolute differential cross sections at 90° in argon as determined in this work from phase-shift analysis and from a relative flow normalization at a steady-state driving pressure are given in Table II together with previous experimental results. Table II shows that the results presented here have a large degree of internal consistency. The phase-shift analysis results, which do not depend upon the previously determined absolute results in helium,[1] agree extremely well with the two relative flow normalizations, which do depend upon such previous results. Furthermore, Table II shows that phase-shift analysis gives valid results in argon in the energy domain used in the present work. Finally, the agreement of the two methods at 15 and 20 eV suggests that a phase-shift analysis may be used to model data at energies at least about twice the inelastic threshold energy. However, it should be noted that the phase shifts derived from such analysis might not have any external validity.

The first four phase shifts determined in this work are presented in Table III together with the previous experimental determinations of Andrick,[3] Williams,[4] and Srivastava *et al.*,[5] and the calculations of Fon *et al.*,[13] McEachran and Stauffer,[14] and Ali and Fraser.[15] The phase shifts determined in this work are in general agreement with the results of Andrick,[3] Williams,[4] Srivastava *et al.*,[5] Fon *et al.*,[13] McEachran and Stauffer,[14] and Ali and Fraser,[15] at 3, 5, and 10 eV. At 15 eV, while the present results agree with those of Andrick,[3] Williams,[4] Fon *et al.*,[13] McEachran and Stauffer,[14] and Ali and Fraser,[15] there are differences between the present results and those of Srivastava *et al.*[5] that are outside the error limits of the present results. At 20 eV, the present results show markedly different values for each of the fitted

TABLE II. Absolute e^--Ar differential scattering cross sections at 90° in units of 10^{-20} m^2/sr.

Energy	Present results				Srivastava *et al.*[c]	
(eV)	PSA	RFN	Andrick[a]	Williams[b]	PSA	RFN
3	0.57±0.09	0.57±0.08	0.64	0.68	0.63	0.62
5	0.87±0.08	0.91±0.1	0.94		0.97	0.82
10	0.97±0.06	1.02±0.12	1.01	1.12	1.11	0.78
15	0.54±0.04	0.49±0.06	0.56	0.58	0.57	0.62
20	0.29±0.02	0.34±0.04	0.45	0.38	0.51	0.38

[a]Reference 3.
[b]Reference 46.
[c]Reference 5.

TABLE III. First four phase shifts in Ar as determined by various investigators.

Energy	δ_0	δ_1	δ_2	δ_3	Work
3	$-0.488(^{+8.2\%}_{-8.6\%})$	$-0.124(^{+9.8\%}_{-9.9\%})$	$0.102(^{+12.3\%}_{-13.6\%})$	$0.025(^{+20.1\%}_{-25.5\%})$	Present
	−0.493	−0.142	0.120	0.025	Reference 3
	−0.457	−0.134	0.142	0.021	Reference 4
	−0.548	−0.140	0.125	0.035	Reference 5
	−0.487	−0.148	0.113	0.026	Reference 13
	−0.472	−0.117	0.128	0.025	Reference 14
	−0.481	−0.105	0.130	0.026	Reference 15
				0.024	Reference 12
5	$-0.770(^{+3.1\%}_{-3.5\%})$	$-0.277(^{+4.8\%}_{-4.5\%})$	$0.228(^{+7.8\%}_{-6.7\%})$	$0.044(^{+17.1\%}_{-18.0\%})$	Present
	−0.733	−0.277	0.260	0.044	Reference 3
	−0.747	−0.256	0.254	0.031	Reference 5
	−0.732	−0.298	0.244	0.043	Reference 13
	−0.709	−0.25	0.312	0.043	Reference 14
	−0.721	−0.246	0.258	0.044	Reference 15
				0.041	Reference 12
10	$-1.08(^{+2.8\%}_{-2.6\%})$	$-0.650(^{+3.3\%}_{-3.9\%})$	$0.720(^{+5.1\%}_{-4.6\%})$	$0.071(^{+11.2\%}_{-12.5\%})$	Present
	−1.143	−0.562	0.842	0.100	Reference 3
	−1.098	−0.528	0.936	0.093	Reference 4
	−1.243	−0.430	0.805	0.171	Reference 5
	−1.155	−0.587	0.757	0.085	Reference 13
	−1.128	−0.541	1.104	0.099	Reference 14
	−1.144	−0.538	0.754	0.100	Reference 15
				0.081	Reference 12
15	$-1.44(^{+2.6\%}_{-3.0\%})$	$-0.830(^{+4.8\%}_{-4.5\%})$	$1.24(^{+4.0\%}_{-3.9\%})$	$0.119(^{+16.0\%}_{-17.0\%})$	Present
	−1.443	−0.782	1.390	0.145	Reference 3
	−1.394	−0.750	1.451	0.154	Reference 4
	−1.365	−0.506	1.593	0.200	Reference 5
	−1.452	−0.789	1.311	0.135	Reference 13
	−1.422	−0.751	1.632	0.163	Reference 14
	−1.442	−0.757	1.196	0.165	Reference 15
				0.122	Reference 12
20	$-2.09(^{+3.8\%}_{-3.3\%})$	$-1.485(^{+7.9\%}_{-8.1\%})$	$1.071(^{+6.6\%}_{-6.0\%})$	$0.129(^{+35.2\%}_{-19.6\%})$	Present
	−1.683	−0.962	1.670	0.232	Reference 3
	−1.653	−0.935	1.747	0.241	Reference 4
	−1.818	−0.871	1.679	0.262	Reference 5
	−1.653	−0.918	1.837	0.231	Reference 14
	−1.674	−0.930	1.440	0.233	Reference 15
				0.162	Reference 12

TABLE IV. Total cross sections determined by various investigators in units of 10^{-20} m^2/sr.

(eV)	Present work	Srivastava *et al.*[a] PSA	Srivastava *et al.*[a] RSN	Williams[b]	Andrick[c]	Buckman and Lohmann[d]	Ali and Fraser[e]	McEachran and Stauffer[f]	Fon *et al.*[g]
3.0	5.20	6.67	5.5	5.64	5.74	4.96	5.37	5.37	5.63
5.0	9.42	10.03	8.4	10.10	9.72	8.81	9.19	10.65	9.24
10.0	19.95	20.11	18.0	23.34	21.63	20.06	19.31	27.31	19.94
15.0	23.22	22.28	21.0	23.93	23.92	23.04	22.06	24.29	23.27
20.0	18.60	19.74	12.5	19.77	19.92	18.30	19.91	19.18	

[a]Reference 5.
[b]Reference 4.
[c]Reference 3.
[d]Reference 10.
[e]Reference 15.
[f]Reference 14.
[g]Reference 13.

phase shifts from each of the previous measurements and calculations.

The total cross sections calculated from the fitted phase shifts, given in Table III, are shown in Table IV. The agreement at all common energies with measurements of Andrick[3] and Buckman and Lohmann,[10] is excellent (about 5% or better). The agreement with the previous results of Williams[4] and Srivastava *et al.*[5] [determined from phase-shift analysis (PSA)] is also quite good (5–15 %). The agreement with the relative flow normalization (RFN) results of Srivastava *et al.*[5] is considerably worse (from 6–40 %). The agreement with the calculations of Fon *et al.*[13] and Ali and Fraser[15] for energies below 20 eV is also excellent. The agreement with the results of McEachran and Stauffer[14] is not quite as good.

The excellent agreement of the present results with the direct determinations of Buckman and Lohmann[10] at 15 and 20 eV indicates that though the use of PSA above threshold with real phase shifts is not strictly valid, such an analysis can give a physically realistic result. One might expect this to become less true as one goes further above threshold. Finally, it should be noted that the agreement between the various total cross-section determinations is generally better than the agreement between the various differential cross-section determinations. This is very likely because the determination of the differential cross sections from their corresponding phase shifts is a more sensitive test of the measurement or calculation.

[1]N. C. Steph, L. McDonald, and D. E. Golden, J. Phys. B **12**, 1507 (1979).
[2]D. E. Golden, J. Furst, and M. Mahgerefteh, Phys. Rev. A **30**, 1247 (1984).
[3]D. Andrick (private communication).
[4]J. F. Williams, J. Phys. B **12**, 265 (1979).
[5]S. K. Srivastava, H. Tanaka, A. Cutjian, and S. Trajmar, Phys. Rev. A **23**, 2156 (1981).
[6]R. D. Dubois and M. E. Rudd, J. Phys. B **9**, 2657 (1976).
[7]T. M. Miller and B. Bederson, Adv. At. Mol. Phys. **13**, 1 (1977).
[8]J. Furst, M. Mahgerefteh, and D. E. Golden, Phys. Rev. A **30**, 2256 (1984).
[9]J. C. Nickel, C. Mott, I. Kanik, and D. C. McCollum, J. Phys. B **21**, 1867 (1988).
[10]S. J. Buckman and B. Lohmann, J. Phys. B **19**, 2547 (1985).
[11]W. H. Press, B. P. Flannery, S. A. Teukolsky, and W. T. Vertterling, *Numerical Recipes: The Art of Scientific Computing* (Cambridge University Press, Cambridge, England, 1986).
[12]T. F. O'Malley, L. Spruch, and L. J. Rosenburg, Math. Phys. **2**, 491 (1961).
[13]W. C. Fon, K. A. Berrington, P. G. Burke, and A. Hibbert, J. Phys. B **16**, 307 (1983).
[14]R. P. McEachran and A. D. Stauffer, J. Phys. B **16**, 4023 (1983).
[15]M. K. Ali and P. A. Fraser, J. Phys. B **10**, 3091 (1977).